

Long-range entanglement near a Kondo-destruction quantum critical point

Christopher Wagner,¹ Tathagata Chowdhury,^{1,2} J. H. Pixley,^{3,4} and Kevin Ingersent¹

¹*Department of Physics, University of Florida, Gainesville, Florida 32611-8440, USA*

²*Institut für Theoretische Physik, Universität zu Köln, Zülpicher Strasse 77a, 507937 Köln, Germany*

³*Department of Physics and Astronomy, Center for Materials Theory, Rutgers University, Piscataway, NJ 08854 USA*

⁴*Condensed Matter Theory Center and the Joint Quantum Institute,*

Department of Physics, University of Maryland, College Park, Maryland 20742-4111, USA

(Dated: March 22, 2018)

The numerical renormalization group is used to study quantum entanglement in the Kondo impurity model with a pseudogapped density of states $\rho(\varepsilon) \propto |\varepsilon|^r$ ($r > 0$) that vanishes at the Fermi energy $\varepsilon = 0$. The model features a Kondo-destruction quantum critical point (QCP) separating a partially screened phase (reached for impurity-band exchange couplings $J > J_c$) from a local-moment phase ($J < J_c$). The impurity contribution S_e^{imp} to the entanglement entropy between a region of radius R around the magnetic impurity and the rest of the host system reveals a characteristic length scale R^* that distinguishes a regime $R \ll R^*$ of maximal critical entanglement from one $R \gg R^*$ of weaker entanglement. Within each phase, S_e^{imp} is a universal function of R/R^* with a power-law decay for $R/R^* \gg 1$. The entanglement length scale R^* diverges on approach to the QCP with a critical exponent that depends only on r .

Advances in quantum information have led to the quantification of entanglement [1], which has helped develop new fundamental concepts in condensed matter physics [2]. The entanglement entropy S_e characterizes the entanglement of a pure state of a system with respect to a partition into two subsystems A and B . If $S_e > 0$, then a measurement that collapses the state of A will also collapse the state in B , whereas if $S_e = 0$, such a measurement on A will not affect B . The entanglement of a subsystem has recently been measured in ultra-cold atomic gases [3], making it experimentally relevant to ask how the entanglement scales with the length l of the smaller subsystem in d spatial dimensions. Certain eigenstates can be classified by an “area law” $S_e \sim l^{d-1}$ (applicable, e.g., to various ground states [4]) or by a “volume law” $S_e \sim l^d$ (typical for highly excited states in a thermal system [5]). The existence of a Fermi surface can impart a logarithmic correction to the area law for ground states of fermionic systems at finite density, i.e., $S_e \sim l^{d-1} \log l$ [6]. In more exotic phases that lack a local order parameter, $S_e = al - \gamma + \dots$ describes a long-range-entangled ground state with a universal area-law offset γ due to topological order in $d = 2$ [7, 8].

Entanglement entropy has been particularly successful at characterizing the ground states of quantum impurity models, in which a local dynamical degree of freedom can be screened via entanglement with a dense set of host energy levels. For example, the Kondo effect is an inherently quantum-mechanical phenomenon due to its singlet ground state [9]. It is therefore natural to expect that the size of the Kondo screening cloud dictates the spatial range of entanglement, a picture that has been confirmed for an interacting spin chain described by the same effective low-energy theory as the Kondo model [10, 11]. However, a direct observation in the degrees of freedom of the original model has hitherto been lacking. Moreover, in situations where the Kondo effect can be driven critical at a continuous quantum phase transition [12–

26], the fate of the Kondo screening cloud and the spatial structure of entanglement are both poorly understood. Is entanglement long ranged at a Kondo-destruction quantum critical point (QCP), despite the impurity becoming asymptotically free at low temperatures? This question is relevant for certain heavy-fermion compounds—such as $\text{CeCu}_{6-x}\text{Au}_x$ [27], YbRh_2Si_2 [28] and CeRhIn_5 [29]—that are believed to exhibit a Kondo-destruction QCP concomitant with a jump in the Fermi-surface volume. Entanglement entropy can provide crucial insights into the nature of the many-body ground state near such a bulk QCP.

In this Letter, we show that the numerical renormalization group (NRG) can be used to accurately calculate the entanglement in the ground state of a spin- $\frac{1}{2}$ magnetic impurity in a metallic or semimetallic host. Previously, we have investigated the “local” entanglement between such an impurity and its host, taking the impurity alone to form subsystem A [26]. Here, we instead compute $S_e^{\text{imp}}(R)$, the impurity contribution to the entanglement entropy between a region of radius R about the impurity site and the rest of the system. For a metal, where the impurity spin becomes fully screened at temperatures $T \ll T_K$ (the Kondo temperature), we directly confirm the previously deduced [10, 11] scaling of S_e^{imp} with R/R_K , where $R_K \propto 1/T_K$ is believed to be the characteristic size of the many-body Kondo screening cloud.

Our main results are for the pseudogap Kondo model [12], which features a Kondo-destruction QCP at an impurity-band exchange coupling $J = J_c$ separating a partially screened Kondo phase ($J > J_c$) from a local-moment phase ($J < J_c$) in which there is no *static* Kondo effect. Each phase reveals a length scale R^* such that for $R \ll R^*$, S_e^{imp} takes its maximal value, a signature of strong entanglement associated with the QCP. In the Kondo phase, S_e^{imp} decreases for $R \gg R^*$, but (in contrast to the conventional metallic case) remains nonzero even for $R \rightarrow \infty$ due to the incomplete screening of the

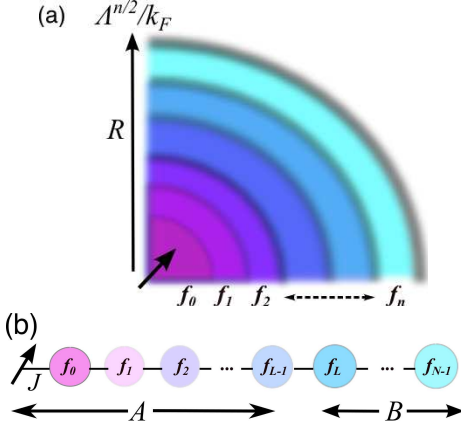


FIG. 1. NRG representation of the Kondo model as a tight-binding Wilson chain of N sites coupled at one end to an impurity spin. (a) In real space, Wilson site n corresponds to a spherically symmetric band state with a radial probability density peaked at a radius $\propto k_F^{-1} \Lambda^{n/2}$ from the impurity. (b) The entanglement entropy $S_e(J, L, N)$ is found by splitting the mapped system into subsystems A (the impurity and the first L Wilson sites) and B (the remaining $N - L$ sites).

impurity [14]. In the local-moment phase, the strong entanglement for $R \ll R^*$ evidences a *dynamical* Kondo effect, but S_e^{imp} drops toward zero for $R \gg R^*$. In both phases, S_e^{imp} obeys universal scaling in terms of R/R^* with a power-law decay for $R/R^* \gg 1$ described by a non-integer exponent. On approach to the QCP, the entanglement length diverges like $R^* \sim |J - J_c|^{-\nu}$, leading to a maximal, scale-invariant entanglement extending from the impurity throughout the entire system.

Model. We consider the spin- $\frac{1}{2}$ Kondo Hamiltonian

$$H = \sum_{\mathbf{k}, \sigma} \varepsilon_{\mathbf{k}} c_{\mathbf{k}\sigma}^\dagger c_{\mathbf{k}\sigma} + \frac{J}{2N_{\mathbf{k}}} \mathbf{S}_{\text{imp}} \cdot \sum_{\mathbf{k}, \mathbf{k}', \sigma, \sigma'} c_{\mathbf{k}\sigma}^\dagger \boldsymbol{\sigma}_{\sigma\sigma'} c_{\mathbf{k}'\sigma'}, \quad (1)$$

where $c_{\mathbf{k}\sigma}$ destroys a band electron of energy $\varepsilon_{\mathbf{k}}$ and spin z component $\sigma = \pm \frac{1}{2}$, $N_{\mathbf{k}}$ is the number of \mathbf{k} values (i.e., the number of host unit cells), J is the local exchange coupling between band electrons and the impurity spin \mathbf{S}_{imp} , and $\boldsymbol{\sigma}$ is a vector of Pauli matrices. We consider a density of states of the (highly simplified) form

$$\rho(\varepsilon) = N_{\mathbf{k}}^{-1} \sum_{\mathbf{k}} \delta(\varepsilon - \varepsilon_{\mathbf{k}}) = \rho_0 |\varepsilon/D|^r \Theta(D - |\varepsilon|), \quad (2)$$

where D is the half-bandwidth and $\Theta(x)$ is the Heaviside function. The model has a rich phase diagram that crucially depends on the band exponent r [14]. The case $r = 0$ corresponds to the conventional Kondo problem in a metal [9]. For semimetals with $0 < r < \frac{1}{2}$, the above-mentioned Kondo-destruction QCP occurs at $J = J_c > 0$. At this interacting QCP, the system exhibits a critical impurity spin response characterized by nontrivial, r -dependent exponents [15].

We consider the impurity-induced change in the entanglement entropy, defined as $S_e^{\text{imp}}(J, R) \equiv S_e(J, R) -$

$S_e^{(0)}(R)$. Here, $S_e(J, R)$ is the entanglement entropy of the combined impurity-band system with subsystem A consisting of the impurity plus that part of the band within radius R of the impurity site, and $S_e^{(0)}(R)$ is the entanglement entropy of the band alone when partitioned at the same radius R [see Fig. 1(a)]. Since the exchange coupling in Eq. (1) is spherically symmetric, the impurity affects only the s -wave band degrees of freedom, and for purposes of calculating impurity-induced properties, the problem reduces to one (radial) dimension. After this reduction, one has [6, 30, 31] $S_e^{(0)}(R) \sim \log R$ rather than the full three-dimensional behavior $S_e^{(0)}(R) \sim R^2 \log R$.

Computational method. We study the radial Kondo model using the NRG [32, 33] as modified to treat a power-law density of states [14]. The Hamiltonian is mapped onto a semi-infinite tight-binding “Wilson chain” of sites labeled $n = 0, 1, 2, \dots$, coupled to the impurity via site 0 only. A discretization parameter $\Lambda > 1$ introduces a separation of energy scales that causes the nearest-neighbor hopping coefficients to decay exponentially as $t_n \sim D \Lambda^{-n/2}$ and allows iterative diagonalization of Kondo Hamiltonians H_M having finite Wilson chains of length M with $M = 1, 2, \dots, N$.

To quantify entanglement, the system described by H_N is divided into a subsystem A comprising the impurity and the first L chain sites ($0 \leq n \leq L - 1$) and a subsystem B containing the remaining chain sites ($L \leq n \leq N - 1$) [see Fig. 1(b)]. We obtain the entanglement entropy $S_e(J, L, N) = -\text{Tr}_A(\rho_A \ln \rho_A)$ by using the NRG solutions of H_M with $L - 1 \leq M \leq N$ to compute the reduced density operator for subsystem A : $\rho_A = \text{Tr}_B(\rho)$ [34–37]. Here, $\rho \propto \exp(-H_N/k_B T)$ is the density operator at a thermal energy scale $k_B T \sim t_N$, chosen to be much smaller than any other energy of physical interest so that the ground-state entanglement is calculated. (For $J < J_c$, a tiny magnetic field is introduced to remove a spurious contribution to S_e from the two-fold ground-state degeneracy [26].) We also calculate the entanglement entropy $S_e^{(0)}(L, N)$ for the same partition of the chain but without the impurity [37]. The impurity entanglement entropy, defined as $S_e^{\text{imp}}(J, L, N) = S_e(J, L, N) - S_e^{(0)}(L, N)$, is independent of N provided that $N \gg L$, but shows an alternating term proportional to $(-1)^L$ that decays only slowly with increasing L [10, 38]. We therefore focus on a smoothed three-point average $S_e^{\text{imp}}(J, L) = \lim_{N \gg L} [S_e^{\text{imp}}(J, L - 1, N) + 2S_e^{\text{imp}}(J, L, N) + S_e^{\text{imp}}(J, L + 1, N)]/4$ [37].

To find S_e as a function of physical distance R from the impurity, we note that site n of the Wilson chain is associated with a single-electron wave function $\psi_n(r')$ that has its greatest radial probability density at radius $r'_n \simeq c \Lambda^{n/2}/k_F$, where k_F is the Fermi wave vector and c is a dimensionless constant of order unity [39] [see Fig. 1(a)]. In the physical limit $N \rightarrow \infty$ and $\Lambda \rightarrow 1$, $\psi_n(r')$ approaches a radial delta function. Even for $\Lambda > 1$, we expect the smoothed entanglement entropy $S_e^{\text{imp}}(J, L)$ to reasonably approximate its continuum counterpart

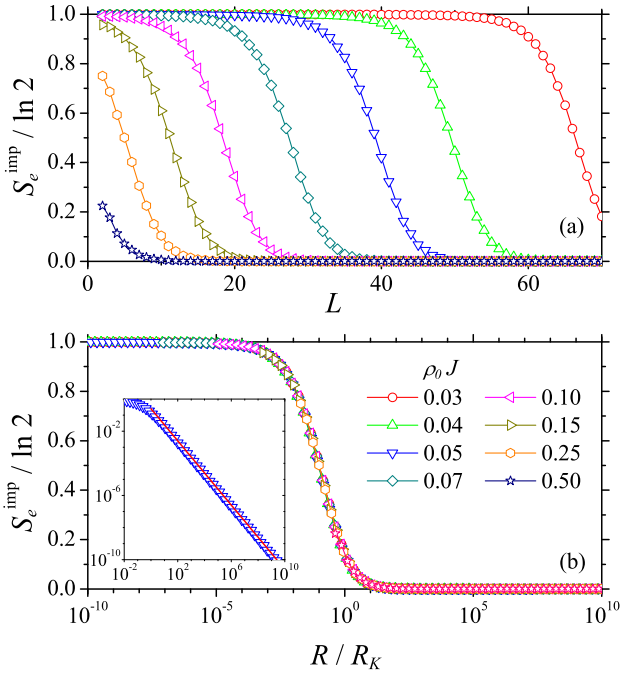


FIG. 2. (a) Impurity entanglement entropy S_e^{imp} vs Wilson chain partition size L for a metallic host ($r = 0$) and different Kondo couplings J labeled in the legend of (b). Lines are guides to the eye. (b) Data from (a) replotted as S_e^{imp} vs R/R_K , where $R = cL^{L/2}/k_F$ and $R_K = 1/(k_F T_K)$ with T_K being the Kondo temperature extracted from the magnetic susceptibility [37]. The collapse of data for different J values points to a one-parameter scaling $S_e^{\text{imp}}(J, R) = f_0(R/R_K)$. Inset: Data from main panel for $\rho_0 J = 0.05$ replotted on a log-log scale showing an $(R/R_K)^{-1}$ tail (fitted line) for $R \gg R_K$.

$S_e^{\text{imp}}(J, R = c\Lambda^{L/2}/k_F)$. We present results obtained using discretization parameter $L = 3$, retaining up to 600 many-body eigenstates after each NRG iteration to reach a Wilson chain of $N = 161$ sites. We employ the conventional NRG value $c = 2L^{1/2}/(L + 1)$ and work in units where $D = \hbar = k_B = g\mu_B = 1$ [37].

Results for a metallic host. First we consider the conventional Kondo model described by band exponent $r = 0$. Figure 2(a) plots the impurity entanglement entropy S_e^{imp} vs L for eight values of the Kondo coupling J . For all but the largest J values, S_e^{imp} starts for small L at the value $\ln 2$ indicative of a singlet formed between (i) a spin $\frac{1}{2}$ arising from an impurity that is negligibly screened by electrons occupying Wilson sites $n < L$, and (ii) a net spin $\frac{1}{2}$ representing the part of the Kondo screening cloud residing on Wilson chain sites $n \geq L$. For large L , S_e^{imp} approaches zero from above, indicating that the impurity is being Kondo-screened almost entirely by electrons within subsystem A , leaving an entanglement with subsystem B no greater than in the absence of the impurity.

It is natural to associate the crossover from $S_e^{\text{imp}} \simeq \ln 2$ to $S_e^{\text{imp}} = 0$ with the renormalization-group (RG) flow

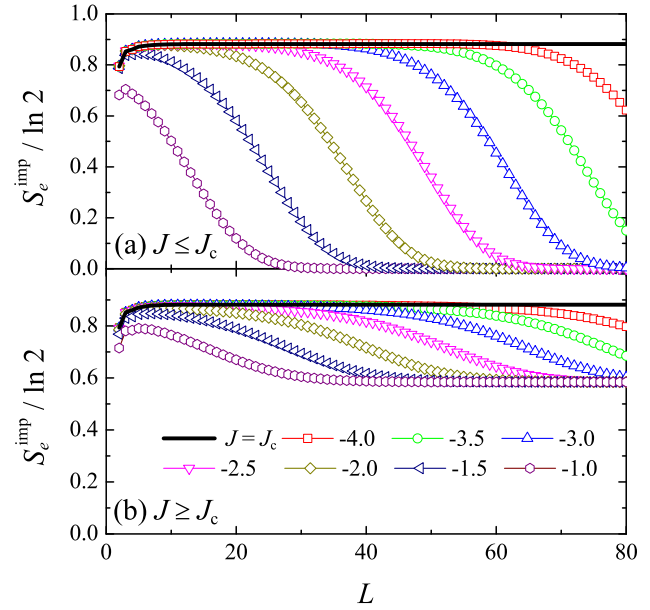


FIG. 3. Impurity entanglement entropy S_e^{imp} vs Wilson chain partition size L for a pseudogap Kondo model with band exponent $r = 0.4$. Symbols plot data for (a) $J = (1 - 10^x)J_c$, and (b) $J = (1 + 10^x)J_c$, with values of x shown in the legend. Thick lines show the critical case $J = J_c$.

from weak to strong coupling, known from much previous work [9] to be characterized by a single energy scale T_K . Accordingly, the entanglement is believed [10] to have just one length scale $R_K \simeq 1/(k_F T_K)$. Figure 2(b) replots data from Fig. 2(a) as S_e^{imp} vs R/R_K , revealing an excellent collapse of results for different J and pointing to the existence of a universal scaling $S_e^{\text{imp}}(J, R) = f_0(R/R_K)$. For $R/R_K \gg 1$, S_e^{imp} decays like $(R/R_K)^{-1}$ [see inset to Fig. 2(b)], consistent with studies of spin chains [10] and a resonant-level model [40].

Results for pseudogapped hosts. Our main interest is in the entanglement near the Kondo-destruction QCPs that occur for semimetallic densities of states described by exponents $0 < r < \frac{1}{2}$. Figure 3 illustrates for $r = 0.4$ the variation of S_e^{imp} with Wilson chain partition size L for values of J close to J_c . In the local-moment phase [Fig. 3(a)], S_e^{imp} initially rises with increasing L to reach a plateau maximum, only to fall toward zero for larger partition sizes. These data show that even though the impurity spin asymptotically decouples from the band, the impurity induces additional entanglement for finite values of L —or equivalently, at finite energies $\simeq \pm DL^{-L/2}$ —manifesting a *dynamical Kondo effect*.

In the Kondo phase, too, S_e^{imp} initially rises with increasing L to reach the same plateau maximum as for $J < J_c$, before decreasing for larger L values [Fig. 3(b)]. Here, however, the impurity induces an additional entanglement that remains nonzero as $L \rightarrow \infty$. This is consistent with the nonvanishing $T \rightarrow 0$ limits of both

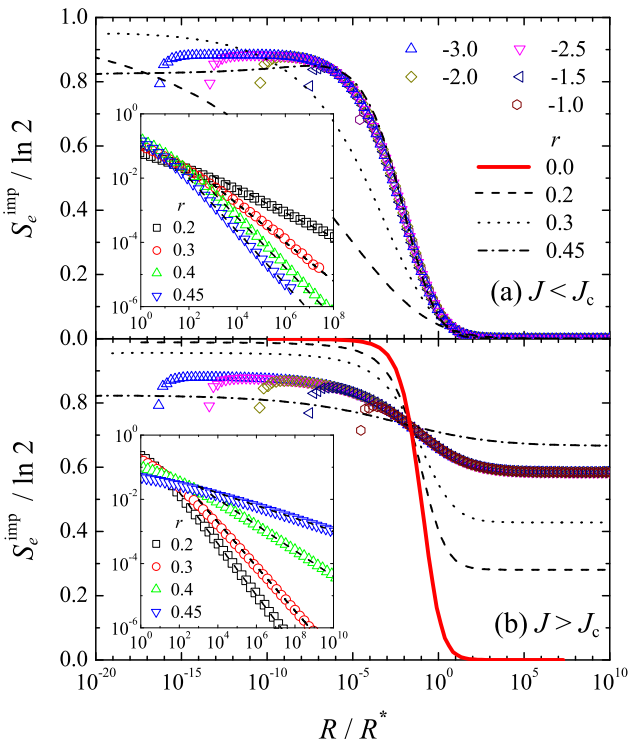


FIG. 4. Data from Fig. 3 replotted vs R/R^* , where $R \propto L^{L/2}/k_F$ and $R^* = 1/(k_F T^*)$ with T^* being a crossover temperature extracted from the magnetic susceptibility [37]. Symbols plot data for (a) $J = (1 - 10^x)J_c$, and (b) $J = (1 + 10^x)J_c$ with values of x labeled in the legend. Lines show fits to data points (not shown) obtained for other values of r . Insets: Log-log plots of large- R data for $S_e^{\text{imp}}(J, R) - S_e^{\text{imp}}(J, \infty)$ vs R/R^* , calculated for a single Kondo coupling (a) $J < J_c$, (b) $J > J_c$ at each of four different band exponents $r > 0$, with power-law fits (dashed lines).

the impurity entropy and the effective magnetic moment, which suggest that the impurity degree of freedom is only partially screened in the pseudogap Kondo phase [14].

Figure 3 also shows that in either phase, S_e^{imp} remains near its initial plateau to larger values of L the closer J approaches J_c . We are thus led to one of our principal conclusions: At the QCP [thick lines in Figs. 3(a) and 3(b)], the *entire* conduction band is maximally entangled with the impurity, i.e., the ground state has long-range, scale-invariant entanglement.

The preceding picture implies that the eventual decrease in S_e^{imp} vs L seen for $J \neq J_c$ reflects the RG flow away from the pseudogap Kondo QCP, a flow characterized by a crossover temperatures scale $T^* \sim |J - J_c|^\nu$, where $\nu(r)$ is the correlation-length exponent [15]. Following the same reasoning as was applied for a metallic ($r = 0$) host, we expect T^* to be associated with a length scale $R^* = 1/(k_F T^*)$. Figure 4 replots the $r = 0.4$ data from Fig. 3 as S_e^{imp} vs R/R^* using values of T^* extracted from the magnetic susceptibility [14, 37]. The scaling collapse of data for different J is of a similar quality to that

for $r = 0$ [see Fig. 2(b)]. This provides strong evidence for the existence of scaling functions f_r^\pm such that

$$S_e^{\text{imp}}(J, R) = f_r^\pm(R/R^*) \quad \text{for} \quad J \gtrless J_c. \quad (3)$$

Significant departures from scaling are seen only for the smallest values of R (corresponding to the smallest L in Fig. 3), and can be attributed to the NRG discretization. Figure 4 also plots fitting curves from similar data collapses for band exponents $r = 0.2$, $r = 0.3$ and $r = 0.45$ [41], as well as [in panel (b)] the metallic case $r = 0$.

Whereas in the local-moment phase $S_e^{\text{imp}} \rightarrow 0$ for $R/R^* \rightarrow \infty$, in the Kondo phase S_e^{imp} approaches for $R/R^* \gg 1$ a value that is well-approximated by $S_e^{\text{imp}} \simeq \frac{3}{2}r \ln 2$ [37]. Insets in Fig. 4 show that in either phase, the impurity entanglement entropy has a power-law tail

$$S_e^{\text{imp}}(J, R) - S_e^{\text{imp}}(J, \infty) \propto (R/R^*)^{-\alpha} \quad \text{for} \quad R \gg R^*. \quad (4)$$

Fitted exponents are consistent with $\alpha = 2r$ for $J < J_c$ and $\alpha = \min(1-r, 2-4r)$ for $J > J_c$, values that represent twice the dimension of the leading irrelevant operator at the local-moment and Kondo fixed points, respectively [37]. This observation is consistent with the interpretation that the power-law tails are associated with the RG flow toward a stable fixed point.

Discussion. We have determined the spatial structure of entanglement entropy in two types of quantum impurity models. Our work demonstrates that the impurity entanglement entropy for a system partitioned at radius R around a Kondo impurity depends only on R divided by $R^* \propto 1/T^*$, where T^* is a many-body scale. In the conventional case of a metallic host, T^* is the Kondo temperature, whereas T^* vanishes like $|J - J_c|^\nu$ on approach to the Kondo-destruction critical point in a pseudogapped host. The impurity entanglement entropy is both scale invariant and long ranged at this interacting critical point, while away from criticality it falls off like $\sim (R/R^*)^{-\alpha}$ for $R \gg R^*$. We deduce that the *total* entanglement entropy goes like $S_e(J, R) \simeq b \log R + f_r^\pm(R/R^*)$. Our conclusions have been reached for a model [Eqs. (1) and (2)] exhibiting strict particle-hole symmetry, but we expect similar conclusions to apply at the asymmetric interacting QCPs that arise for $0.375 \lesssim r < 1$ upon the addition of a potential-scattering term to Eq. (1) [14].

Although obtained for a single impurity, our results shed light on the Kondo lattice model and have implications for interpretation of experiments on quantum-critical heavy-fermion compounds. First, this work provides insight into the structure of the ground-state wave function in a Kondo-destroyed phase. Even though static screening is suppressed, a dynamical Kondo effect still produces entanglement extending over a length scale that diverges on approach to the Kondo phase boundary. Thus, the ground state of the Kondo lattice cannot be adequately described merely in terms of a static slave-boson amplitude; dynamical effects must be taken into account. Second, our findings suggest that the Kondo-breakdown QCP relevant to heavy-fermion metals is accompanied by

long-range entanglement between all local moments and the entire conduction band. We believe that this scale-invariant entanglement is intimately associated with the reconstruction of the critical Fermi surface.

Acknowledgments. We thank Andreas Ludwig and Andrew Mitchell for useful discussions. This work was sup-

ported in part by NSF Grant No. DMR-1508122 (C.W., T.C., and K.I.), by the DFG within the CRC 1238 (Project C03), and by the Laboratory for Physical Sciences (J.H.P.). The work of K.I. was performed in part at the Aspen Center for Physics, which is supported by NSF Grant No. PHY-1066293.

[1] D. Janzing, in *Compendium of Quantum Physics*, ed. by D. Greenberger, K. Hentschel, and F. Weinert (Springer Berlin Heidelberg, Berlin, Heidelberg, 2009), pp. 205–209.

[2] L. Amico, R. Fazio, A. Osterloh, and V. Vedral, *Rev. Mod. Phys.* **80**, 517 (2008).

[3] R. Islam *et al.*, *Nature* **528**, 77 (2015).

[4] J. Eisert, M. Cramer, and M. B. Plenio, *Rev. Mod. Phys.* **82**, 277 (2010).

[5] R. Nandkishore and D. A. Huse, *Ann. Rev. Condens. Matt. Phys.* **6**, 15 (2014).

[6] D. Gioev and I. Klich, *Phys. Rev. Lett.* **96**, 100503 (2006).

[7] A. Kitaev and J. Preskill, *Phys. Rev. Lett.* **96**, 110404 (2006).

[8] M. Levin and X.G. Wen *Phys. Rev. Lett.* **96**, 110405 (2006). *Nat. Phys.* **7**, 772 (2011).

[9] A. C. Hewson, *The Kondo Problem to Heavy Fermions* (Cambridge Univ. Press, Cambridge, UK, 1993).

[10] E. S. Sørensen, M.-S. Chang, N. Laflorencie, and I. Affleck, *J. Stat. Mech.* **2007**, L01001 (2007).

[11] I. Affleck, N. Laflorencie, and E. S. Sørensen, *J. Phys. A* **42**, 504009 (2009).

[12] D. Withoff and E. Fradkin, *Phys. Rev. Lett.* **64**, 1835 (1990).

[13] R. Bulla, T. Pruschke, and A. C. Hewson, *J. Phys.: Condens. Matt.* **9**, 10463 (1997).

[14] C. Gonzalez-Buxton and K. Ingersent, *Phys. Rev. B* **57**, 14254 (1998).

[15] K. Ingersent and Q. Si, *Phys. Rev. Lett.* **89**, 076403 (2002).

[16] L. Fritz and M. Vojta, *Phys. Rev. B* **70**, 214427 (2004).

[17] M. T. Glossop, S. Kirchner, J. H. Pixley, and Q. Si, *Phys. Rev. Lett.* **107**, 076404 (2011).

[18] I. Schneider, L. Fritz, F. B. Anders, A. Benlagra, and M. Vojta, *Phys. Rev. B* **84**, 125139 (2011).

[19] J. H. Pixley, S. Kirchner, K. Ingersent, and Q. Si, *Phys. Rev. Lett.* **109**, 086403 (2012).

[20] A. M. Sengupta, *Phys. Rev. B* **61**, 4041 (2000).

[21] L. Zhu and Q. Si, *Phys. Rev. B* **66**, 024426 (2002).

[22] G. Zaránd and E. Demler, *Phys. Rev. B* **66**, 024427 (2002).

[23] M. Kirćan and M. Vojta, *Phys. Rev. B* **69**, 174421 (2004).

[24] M. T. Glossop and K. Ingersent, *Phys. Rev. Lett.* **95**, 067202 (2005).

[25] M. T. Glossop and K. Ingersent, *Phys. Rev. B* **75**, 104410 (2007).

[26] J. H. Pixley, T. Chowdhury, M. T. Miecnikowski, J. Stephens, C. Wagner, and K. Ingersent, *Phys. Rev. B* **91**, 245122 (2015).

[27] A. Schröder *et al.*, *Nature* **407**, 351 (2000).

[28] S. Paschen *et al.*, *J. Magn. Magn. Mat.* **400**, 17 (2016).

[29] H. Shishido, R. Settai, H. Harima, and Y. Onuki, *J. Phys. Soc. Jpn.* **74**, 1103 (2005).

[30] B. Swingle, *Phys. Rev. Lett.* **105**, 050502 (2010).

[31] W. Ding, A. Seidel, and K. Yang, *Phys. Rev. X* **2**, 011012 (2012).

[32] K. G. Wilson, *Rev. Mod. Phys.* **47**, 773 (1975).

[33] R. Bulla, T. A. Costi, and T. Pruschke, *Rev. Mod. Phys.* **80**, 395 (2008).

[34] A. Weichselbaum and J. von Delft, *Phys. Rev. Lett.* **99**, 076402 (2007).

[35] L. Merker, A. Weichselbaum, and T. A. Costi, *Phys. Rev. B* **86**, 075153 (2012).

[36] H. T. M. Nghiem and T. A. Costi, *Phys. Rev. B* **90**, 035129 (2014).

[37] See the Supplemental Material at [URL will be provided by publisher] for technical details and additional results.

[38] Reference 26 studied $S_e^{\text{imp}}(J, 0, N)$, which is not directly comparable with the extrapolation to $L = 0$ of the smoothed quantity $S_e^{\text{imp}}(J, L)$ discussed in this work.

[39] H. R. Krishna-murthy, J. W. Wilkins, and K. G. Wilson, *Phys. Rev. B* **21**, 1003 (1980).

[40] H. Saleur, P. Schmitteckert, and R. Vasseur, *Phys. Rev. B* **88**, 085413 (2013).

[41] For $r = 0.2$ and 0.3, the crossover in S_e^{imp} between its critical and stable fixed-point values is centered at smaller R/R^* for $J < J_c$ than for $J > J_c$. This is an artifact of an impurity magnetization $\langle S_{\text{imp}}^z \rangle \sim |h|^{1/\delta}$ induced near $J = J_c$ by the small magnetic field h applied to lift the local-moment ground-state degeneracy. In our quadruple-precision runs, the smallest field that we can use is $h = O(10^{-34})$. For $r = 0.2$, e.g., $1/\delta = 0.026$ gives a non-negligible $\langle S_{\text{imp}}^z \rangle \simeq 0.13$. For $J \rightarrow J_c^-$, it is thus impractical to simulate spontaneous symmetry breaking.

Supplemental Material for “Long-range entanglement near a Kondo-destruction quantum critical point”

Christopher Wagner¹, Tathagata Chowdhury^{1,2}, J. H. Pixley^{3,4}, and Kevin Ingersent¹

¹*Department of Physics, University of Florida, Gainesville, Florida 32611-8440, USA*

²*Institut für Theoretische Physik, Universität zu Köln, Zülpicher Strasse 77a, 50937 Köln, Germany*

³*Department of Physics and Astronomy, Center for Materials Theory, Rutgers University, Piscataway, NJ 08854 USA*

⁴*Condensed Matter Theory Center and the Joint Quantum Institute,*

Department of Physics, University of Maryland, College Park, Maryland 20742-4111, USA

(Dated: March 22, 2018)

This document summarizes technical methods and presents results beyond those contained in the main paper. Section I analyzes the Wilson chain—the discretized representation of the conduction band used in numerical renormalization-group (NRG) calculations—in the absence of any impurity degree of freedom. Data are presented for the dependence of the entanglement entropy S_e on the overall chain length, the position of the cut across which the entanglement is computed, the exponent r entering the density of states

$$\rho(\varepsilon) = \rho_0 |\varepsilon|^r \Theta(D - |\varepsilon|), \quad (\text{S1})$$

and the NRG discretization parameter Λ . Section II addresses the many-body Kondo problem created by coupling a Wilson chain to a spin- $\frac{1}{2}$ impurity. A description of the method that we use to calculate the entanglement entropy is followed by details of the entanglement results presented in the main text.

I. ENTANGLEMENT WITHIN THE WILSON CHAIN

This section focuses on the entanglement properties of isolated Wilson chains (without any coupling to an impurity degree of freedom). The quantity of interest is the entanglement entropy $S_e(L)$ for a chain of length N sites that is split into subsystem A comprising sites 0 through $L - 1$ and subsystem B containing sites L through $N - 1$. Although the notation suggests that S_e is a function of L alone, it must be emphasized that in fact it also depends on N , r , and Λ .

A. The Wilson chain

The NRG method [1, 2] uses a discretization parameter $\Lambda > 1$ to divide a conduction band having single-particle energies ε ranging from $-D$ to D into an infinite set of logarithmic bins spanning $D\Lambda^{-(m+1)} < \pm\varepsilon \leq D\Lambda^{-m}$ for $m = 0, 1, 2, \dots$. Within each bin, the band is approximated by a single representative state, namely, the linear combination of the original band states that couples to the impurity. The band Hamiltonian is then mapped via the Lanczos method onto a tight-binding Hamiltonian for a semi-infinite “Wilson chain” of sites labeled $n = 0, 1, 2, \dots$, coupled to the impurity via site 0 only:

$$H \longrightarrow H_{\text{imp}}[f_{0\sigma}, f_{0\sigma}^\dagger] + \sum_{n=1}^{\infty} \sum_{\sigma} t_n \left(f_{n\sigma}^\dagger f_{n-1,\sigma} + \text{H.c.} \right), \quad (\text{S2})$$

where $t_n \sim D\Lambda^{-n/2}$ for $n \gg 1$ [3]. The reader is referred to Ref. 14 for details of the calculation of the coefficients t_n and their large- n asymptotics for the power-law density of states specified in Eq. (S1).

The discretization-induced separation of energy scales t_n allows controlled approximation of the low-energy states of the full Hamiltonian H through iterative solution of finite-chain Hamiltonians

$$H_M = H_{\text{imp}}[f_{0\sigma}, f_{0\sigma}^\dagger] + H_M^{\text{chain}}, \quad (\text{S3})$$

$$H_M^{\text{chain}} = \sum_{n=1}^{M-1} \sum_{\sigma} t_n \left(f_{n\sigma}^\dagger f_{n-1,\sigma} + \text{H.c.} \right), \quad (\text{S4})$$

with $M = 1, 2, \dots, N$. Here, N is chosen to be sufficiently large that t_N (the largest energy scale of the part of the semi-infinite chain that is omitted from H_N) is much smaller than all energy scales of physical interest.

The Wilson chain hopping coefficients converge for $\Lambda \rightarrow 1$ to those for the exact Lanczos mapping of the continuum (“ $\Lambda = 1$ ”) Kondo model. For example, in the case of a metallic density of states [Eq. (S1) with $r = 0$], t_n decreases

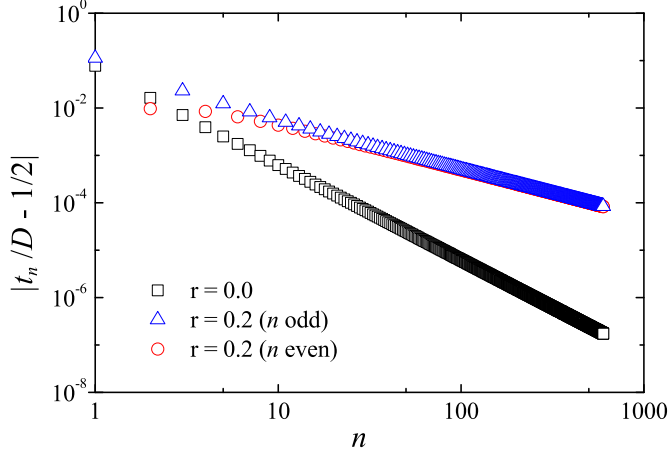


FIG. S1. Tight-binding hopping parameters plotted as $|t_n/D - \frac{1}{2}|$ vs n for the exact Lanczos mapping of a conduction band with a density of states given by Eq. (S1) with $r = 0$ (squares) and $r = 0.2$ (triangles and circles for odd and even n , respectively). Only for $n \rightarrow \infty$ does t_n approach its uniform value $t_n = \frac{1}{2}$ for a standard tight-binding chain.

monotonically from $t_1 \approx 0.57D$ toward $t_\infty = D/2$. The log-log plot in Fig. S1 reveals an exponential decay of $t_n/D - \frac{1}{2}$ with increasing n . This pattern distinguishes the exact tight-binding formulation of the Kondo model from a standard tight-binding (STB) chain corresponding to Eq. (S4) with $t_n = D/2$. The effect of this difference on the entanglement entropy will be discussed below. Figure S1 also plots $|t_n/D - \frac{1}{2}|$ vs n for the pseudogapped case $r = 0.2$. Here t_n for n odd (even) approaches $D/2$ from above (below).

B. Calculation of the entanglement entropy

The entanglement entropy of an isolated Wilson chain (without any impurity coupled to its end) can be computed within the NRG approach in the same manner as the corresponding quantity for the full Kondo problem (see Sec. II A). However, the quadratic nature of H_M^{chain} allows use of a simpler method introduced in Ref. ?, which was used to obtain the results presented in Sec. IC.

The formalism begins with a general fermionic tight-binding Hamiltonian

$$H = \sum_{m,n} t_{mn} c_m^\dagger c_n \quad (\text{S5})$$

having hopping t_{mn} between sites m and n of a finite lattice. We split the system into subsystems A and B , reserving labels i and j for sites within A . In any many-particle eigenstate $|\Psi\rangle$ of H , the single-particle correlation function for subsystem A can be written

$$C_{ij} = \langle \Psi | c_i^\dagger c_j | \Psi \rangle = \text{Tr}_A (\rho_A c_i^\dagger c_j), \quad (\text{S6})$$

where $\rho_A = \text{Tr}_B (|\Psi\rangle\langle\Psi|)$ is the reduced density operator for subsystem A . Given the quadratic form of H , higher correlation functions within A must factorize according to Wick's theorem, and there must exist a Hermitian operator

$$\mathcal{H}_A = \sum_{i,j} \tilde{H}_{ij} c_i^\dagger c_j \quad (\text{S7})$$

such that

$$\rho_A = Z_A^{-1} e^{-\mathcal{H}_A}, \quad Z_A = \text{Tr}_A (e^{-\mathcal{H}_A}). \quad (\text{S8})$$

The matrix \tilde{H}_{ij} has a set of eigenvalues $\tilde{\varepsilon}_k$ and orthonormal eigenvectors \mathbf{v}_k with components v_{ik} that can be used to define new fermionic operators

$$a_k = \sum_i v_{ik}^* c_i \quad \longleftrightarrow \quad c_i = \sum_k v_{ik} a_k \quad (\text{S9})$$

such that

$$\mathcal{H}_A = \sum_k \tilde{\varepsilon}_k a_k^\dagger a_k, \quad \rho_A = Z_A^{-1} \exp\left(-\sum_k \tilde{\varepsilon}_k a_k^\dagger a_k\right), \quad Z_A = \prod_k (1 + e^{-\tilde{\varepsilon}_k}). \quad (\text{S10})$$

Substituting Eq. (S9) into Eq. (S7) yields

$$\tilde{H}_{ij} = \sum_k \tilde{\varepsilon}_k v_{ik} v_{jk}^*, \quad (\text{S11})$$

while substituting Eqs. (S8)–(S10) into Eq. (S6) gives

$$C_{ij} = \sum_k \frac{v_{ik}^* v_{jk}}{e^{\tilde{\varepsilon}_k} + 1}. \quad (\text{S12})$$

Comparison of Eqs. (S11) and (S12) leads to the conclusion that matrices \tilde{H} and C^T (the transpose of C) are diagonalized by the same similarity transformation. We therefore deduce that C^T (and hence C) has eigenvalues

$$\gamma_k = \frac{1}{1 + e^{\tilde{\varepsilon}_k}} \quad \longleftrightarrow \quad \tilde{\varepsilon}_k = \ln(1 - \gamma_k) - \ln \gamma_k. \quad (\text{S13})$$

The entanglement entropy for the partition of the system into subsystems A and B is

$$\begin{aligned} S_e &= -\text{Tr}_A(\rho_A \ln \rho_A) \\ &= \text{Tr}_A(\rho_A \ln Z_A) + \text{Tr}_A \left[Z_A^{-1} \exp\left(-\sum_k \tilde{\varepsilon}_k a_k^\dagger a_k\right) \left(\sum_{k'} \tilde{\varepsilon}_{k'} a_{k'}^\dagger a_{k'}\right) \right] \\ &= \ln Z_A + \prod_k \frac{\tilde{\varepsilon}_k}{e^{\tilde{\varepsilon}_k} + 1} = \sum_k \ln(1 + e^{-\tilde{\varepsilon}_k}) + \sum_k \frac{\tilde{\varepsilon}_k}{e^{\tilde{\varepsilon}_k} + 1} \\ &= \sum_k \ln\left(1 + \frac{\gamma_k}{1 - \gamma_k}\right) + \sum_k \gamma_k [\ln(1 - \gamma_k) - \ln \gamma_k] \\ &= -\sum_k [\gamma_k \ln \gamma_k + (1 - \gamma_k) \ln(1 - \gamma_k)]. \end{aligned} \quad (\text{S14})$$

Equation (S14) provides a computationally fast and accurate method for calculating the entanglement of a spinless Wilson chain or a spinless standard tight-binding chain from the eigenvalues of its single-particle correlation function. To obtain the impurity contribution of the entanglement entropy of the Kondo problem, we subtract twice the entanglement entropy of the spinless chain.

C. Systematics of the Wilson chain entanglement entropy

The entanglement entropy of the Wilson chain exhibits even-odd alternation with increasing size L of partition A . Such an alternation is present for a standard tight-binding chain, but it becomes more pronounced with increasing $\Lambda > 1$ and/or increasing $|r|$. To filter out this alternation, which is a finite-size effect of little interest for our purposes, we consider a three-point average

$$S_e^{\text{avg}}(L) = \frac{1}{4} [S_e(L-1) + 2S_e(L) + S_e(L+1)]. \quad (\text{S15})$$

This section considers first the case of a metallic band with a density of states described by Eq. (S1) with $r = 0$. We identify a range of L values over which S_e^{avg} differs negligibly from the universal dependence exhibited by a standard tight-binding (STB) chain, and describe deviations found for small and large values of L . We then turn to the effects of varying the band exponent r entering Eq. (S1).

Results for $r = 0$: Fig. S2(a) shows the average entanglement entropy S_e^{avg} vs partition length L for a representative case $\Lambda = 1.04$ and for various chain lengths N specified in the legend. $S_e^{\text{avg}}(L)$ is almost (but not quite) symmetric with respect to reflection about $L = N/2$ and peaks very close to $L = N/2$. The value $S_e^{\text{max}} \simeq S_e^{\text{avg}}(N/2)$ initially increases with increasing chain length N , but eventually saturates as a wide plateau forms in $S_e^{\text{avg}}(L)$. No such plateau is observed in the data for $\Lambda = 1$ and $N = 1200$ (plotted with dashed lines).

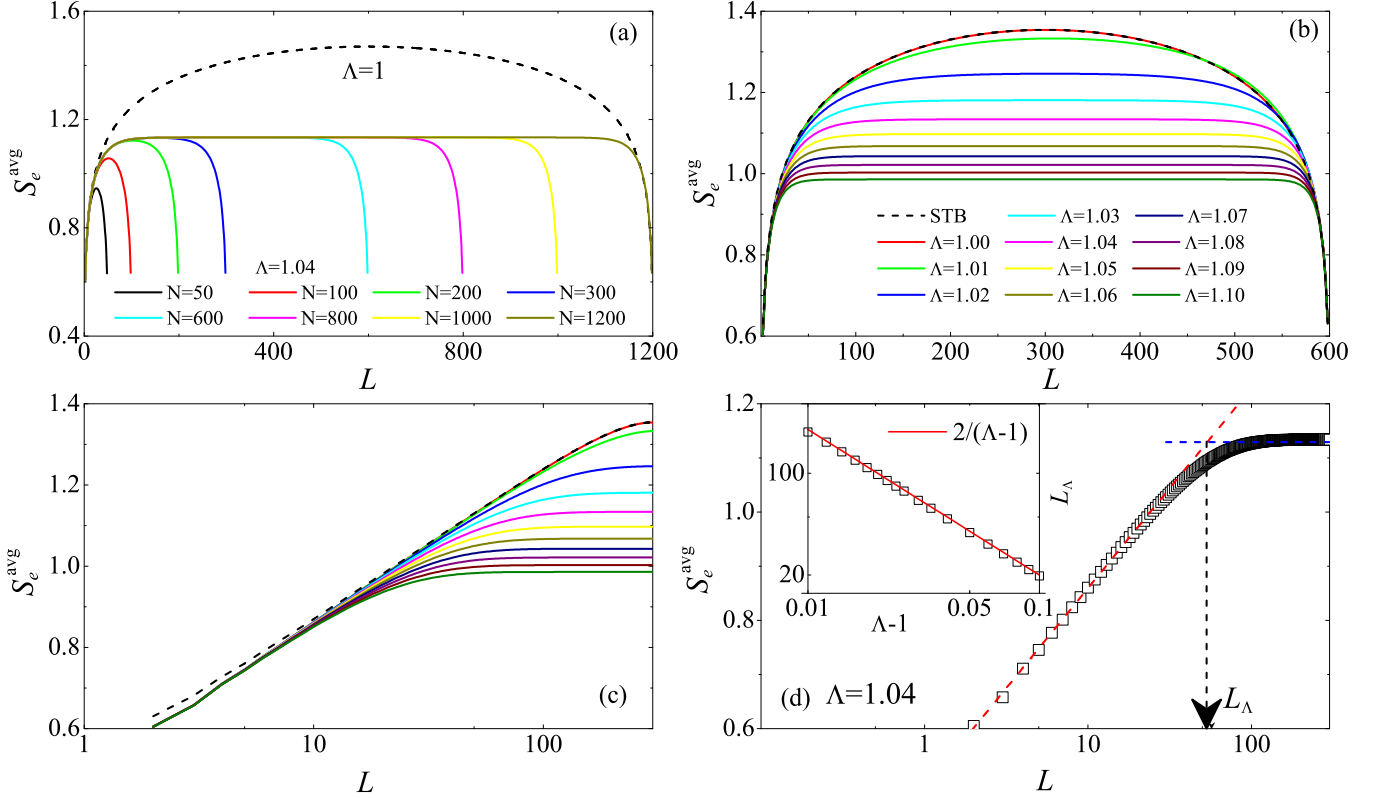


FIG. S2. Wilson chain entanglement entropy S_e^{avg} vs partition size L for a metallic density of states described by Eq. (S1) with $r = 0$. (a) Data for discretization parameter $\Lambda = 1.04$ with different chain lengths N (solid lines), and for $\Lambda = 1$, $N = 1200$ (dashed line). (b) Data for $N = 600$ with different values of Λ (solid lines). Also shown (dashed line) is S_e^{avg} vs partition size L for a 600-site standard tight-binding (STB) chain. (c) Data from (b) replotted vs $\log L$. (d) Data for $N = 600$, $\Lambda = 1.04$ showing the definition of a partition size L_Λ characterizing the crossover from a regime $S_e^{\text{avg}} \sim \log L$ for $L \ll L_\Lambda$ (red dashed line) to a regime $S_e^{\text{avg}} \simeq S_e^{\text{max}}$ for $L \gg L_\Lambda$ (blue dashed line). Inset: L_Λ (calculated for $N = 1200$) vs $\Lambda - 1$ is well approximated by $L_\Lambda = 2/(\Lambda - 1)$ (red line).

Figure S2(b) plots (solid lines) S_e^{avg} vs L for a fixed chain length $N = 600$ and different values of the discretization parameter on the range $1 \leq \Lambda \leq 1.1$. Also shown (dashed line) are the corresponding data for a standard tight-binding (STB) chain with $t_n = D/2$. The STB curve is exactly symmetric about $L = N/2$, while those for Wilson chains are slightly asymmetric. Curves for $\Lambda > 1$ exhibit a plateau similar to that seen in Fig. S2(a). As Λ is increased, the plateau value S_e^{max} decreases and is reached at smaller values of L .

For the fermionic STB chain with constant hopping coefficients between nearest neighbors, the entanglement entropy in the limit $L \ll N$ is equal to that of a critical conformal field theory (CFT) [6]. For a finite system with open boundary conditions,

$$S_e^{\text{avg}} = \frac{c}{6} \ln \left(\frac{N}{\pi} \sin \frac{\pi L}{N} \right) + b \simeq \frac{c}{6} \ln L + b \quad \text{for } L \ll N/2, \quad (\text{S16})$$

where c is the central charge of the CFT and b the boundary entanglement. For a spinless chain, the left-moving and right-moving fermions each carry a charge of $c = 1/2$, so the chain overall is described by $c = 1$. Fig. S2(c) replots the data for $L \leq N/2$ from Fig. S2(b) as S_e^{avg} vs $\log L$. The Wilson chain results (solid lines) can be well approximated by

$$S_e^{\text{avg}} = \begin{cases} \frac{c}{6} \ln L + b & \text{for } 10 \lesssim L \ll L_\Lambda, \\ \frac{c}{6} \ln L_\Lambda + b \equiv S_e^{\text{max}} & \text{for } L_\Lambda \ll L \leq N/2. \end{cases} \quad (\text{S17})$$

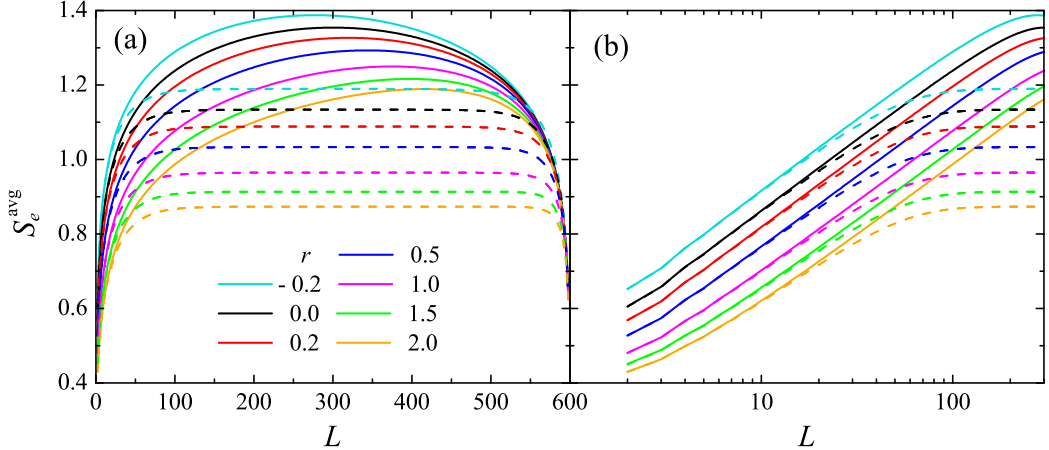


FIG. S3. (a) S_e^{avg} vs L for Wilson chains of length $N = 600$ with different band exponents r , for discretization parameters $\Lambda = 1.0$ (solid lines) and $\Lambda = 1.04$ (dashed lines). (b) Data for $L \leq N/2$ replotted on a logarithmic L scale.

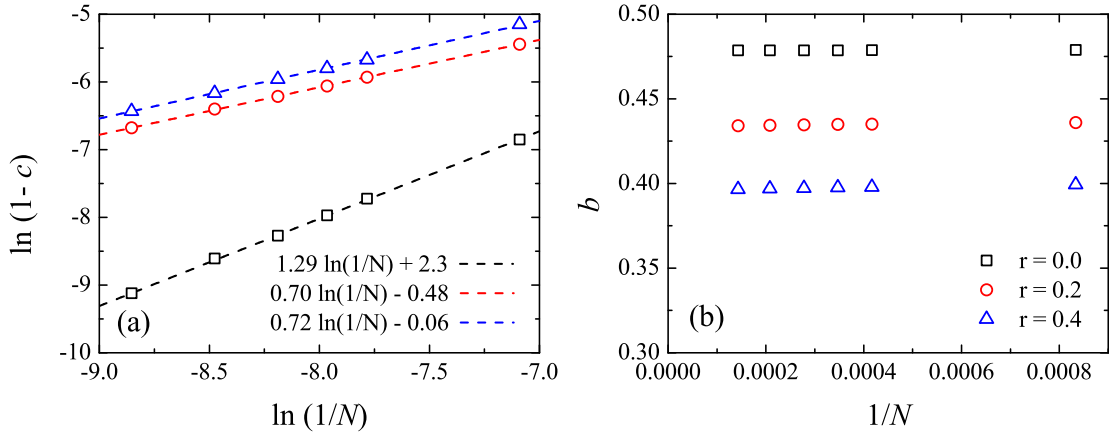


FIG. S4. Fitted coefficients c and b in Eq. (S17) for a Wilson chain with discretization $\Lambda = 1$, and band exponents $r = 0, 0.2$, and 0.4 . (a) Log-log plot of $1 - c$ vs $1/N$, where N is the chain length, showing apparent convergence to $c = 1$ for $1/N \rightarrow 0$. (b) b vs $1/N$.

Here, c and b are independent of Λ and, when extrapolated to the infinite-size limit $1/N \rightarrow 0$, are numerically indistinguishable from their respective STB-chain values: $c = 1$ and $b \simeq 0.478$. For $L \lesssim 10$, all Wilson-chain data coincide but clearly differ from those for the STB chain (dashed line), while the STB and $\Lambda = 1$ Wilson chain entanglement entropies converge for $L \gg 10$. This is unsurprising given the approach with increasing n of the $\Lambda = 1$ Wilson chain hopping coefficients t_n to the STB value $t_n = D/2$ (see Fig. S1).

The scale L_Λ is the focus of Fig. S2(d). The main panel shows how L_Λ can be defined as the horizontal coordinate of the intercept between the small- L and large- L asymptotes defined in Eq. (S17), i.e., $L_\Lambda = \exp[(6/c)(S_e^{\text{avg}} - b)]$. The inset of Fig. S2(d) plots the variation of L_Λ with Λ (data points), demonstrating that for $\Lambda \lesssim 1.1$, the scale is well-described by the empirical relation $L_\Lambda = 2/(\Lambda - 1)$ (line). NRG many-body calculations are typically performed using a discretization parameter on the range $1.5 \leq \Lambda \leq 3$ chosen to balance discretization errors against truncation errors. In all such cases, $L_\Lambda \simeq 1$, so $S_e^{\text{avg}}(L) \simeq S_e^{\text{max}}$ is almost independent of L .

Results for $r \neq 0$: Figure S3 plots S_e^{avg} vs L (panel a) and vs $\log L$ (panel b) for fixed $N = 600$, for $\Lambda = 1$ (solid lines) and $\Lambda = 1.04$ (dashed lines), and for different values of the band exponent r entering Eq. (S1) describing metallic ($r = 0$), pseudogapped ($r > 0$), and divergent ($r < 0$) densities of states. For $\Lambda = 1$, the main effect of increasing $|r|$ is a progressive increase in the asymmetry of $S_e^{\text{avg}}(L)$ about $L = N/2$. As r increases (decreases) from zero, the peak in $S_e^{\text{avg}}(L)$ moves right (left) from $L \simeq N/2$. For $10 \lesssim L \ll N/2$, the entanglement entropy is still described by Eq. (S16), as can be seen from Fig. S3(b). For $\Lambda = 1.04$ (dashed lines in Fig. S3), the entanglement entropy for all r

chain	$c)$	b
STB	1.0000(2)	0.4780(7)
$r = 0$	1.0000(1)	0.47856(5)
$r = 0.2$	1.0000(1)	0.43288(4)
$r = 0.4$	1.0000(1)	0.39500(5)

TABLE I. Values of the coefficients c and b defined in Eq. (S17) for the STB and for Wilson chains with different band exponents r . A number in parentheses denotes the estimated nonsystematic error in the last digit.

values remains consistent with Eq. (S17), where L_Λ is independent of r and the value of S_e^{\max} tracks the r dependence of b , i.e., $S_e^{\max}(r) - S_e^{\max}(0) \simeq b(r) - b(0)$.

Figure S4 plots the variation with inverse chain length $1/N$ of the fitted values of c and b for $\Lambda = 1$ and $r = 0, 0.2$, and 0.4 . Table I lists the result of extrapolating c and b to the long-chain limit $1/N \rightarrow 0$, along with the corresponding values for the STB chain. To within numerical accuracy, the slope remains $c = 1$ independent of r , as demonstrated by a log-log plot of $1 - c$ vs $1/N$ [Fig. S4(a)], whereas the boundary entanglement b decreases (increases) as r is increased (decreased) from zero [Figs. S3(b) and S4(b)].

A density of states of the form of Eq. (S1) describes free fermions in one spatial dimension having a dispersion $\varepsilon \propto |k - k_F|^{1/(1+r)} \text{sgn}(k - k_F)$. It is therefore quite surprising that, apart from a nonuniversal boundary term $b(r)$, the L dependence of S_e^{avg} for $10 \lesssim L \ll N/2$ is the same for $r = 0$ (where the host system exhibits conformal invariance) and for $r \neq 0$ (where the space and time axes are manifestly inequivalent). At present we do not fully understand the physical origin of this result. However, it suggests that the pseudogap host could in fact possess a “hidden” conformal symmetry with a central charge $c = 1$ ($c = \frac{1}{2}$ each for left- and right-movers).

II. ENTANGLEMENT ENTROPY FOR THE PSEUDOGAP KONDO PROBLEM

A. Numerical renormalization-group calculation of entanglement entropy

To calculate the entanglement entropy, we employ the full density-matrix NRG approach [7–9]. In order to explain our method, it is necessary first to briefly review aspects of the conventional NRG approach. If the impurity has d_i internal states (e.g., $d_i = 2$ for a spin $S_{\text{imp}} = \frac{1}{2}$) and each Wilson chain site has d possible states (e.g., $d = 4$ for the single, spinful conduction band considered in the present work), then H_M has a basis of dimension $d_i d^M$. Due to the exponential growth of this dimension with increasing M , starting at some NRG iteration M_0 (typically $M_0 = 5$), the basis must be truncated to keep within acceptable bounds the computational time for setting up and diagonalizing a matrix representation of H_M . The many-body eigenstates of H_M are divided into two sets: the high-energy states $|l, M\rangle$, $1 \leq l \leq n_M^{\text{disc}}$ are discarded, and only the lowest-energy states $|k, M\rangle$, $1 \leq k \leq n_M^{\text{kept}}$ are kept to set up the next Hamiltonian H_{M+1} , which then has a truncated basis of dimension $d n_M^{\text{kept}} \equiv n_{M+1}^{\text{kept}} + n_{M+1}^{\text{disc}}$.

The full density-matrix NRG approach is constructed around a complete basis of dimension $d_i d^N$ for the longest Wilson chain (corresponding to $M = N$). This basis, introduced by Anders and Schiller [10, 11], comprises all states of the form $|l, e, M\rangle = |l, M\rangle \otimes |e, M\rangle$ where M ranges from M_0 (the lowest-numbered iteration at which any eigenstate is discarded) to N (the highest-numbered iteration, and one at which we formally classify every eigenstate as discarded). Here, $|l, M\rangle$ is one of the many-body eigenstates discarded after iteration M and $|e, M\rangle$, called an “environmental state,” is any one of d^{N-M} different possible simple products of basis states for Wilson chain sites M through $N-1$. For any $M < N$, $|l, e, M\rangle$ is not an eigenstate of H_N but the full density-matrix NRG relies on a key approximation that $H_N |l, e, M\rangle \simeq H_M |l, M\rangle = E_{l,M} |l, M\rangle$ (where all energies are measured relative to the ground state of H_N).

Within the complete basis, the thermal equilibrium density matrix for the entire system composed of the impurity and N Wilson chain sites is diagonal and can be written (after tracing out the environmental states)

$$\rho = \begin{pmatrix} \rho_{M_0} & 0 & 0 & 0 \\ 0 & \rho_{M_0+1} & 0 & 0 \\ & & \ddots & \\ 0 & 0 & \rho_{N-1} & 0 \\ 0 & 0 & 0 & \rho_N \end{pmatrix}, \quad (\text{S18})$$

where ρ_M is an $n_M^{\text{disc}} \times n_M^{\text{disc}}$ diagonal matrix having matrix elements

$$(\rho_M)_{ll'} = \sum_{e,e'} \langle l, e, M | \hat{\rho} | l', e', M \rangle = \sum_{e,e'} \delta_{l,l'} \delta_{e,e'} e^{-\beta E_{l,M}} / Z = \delta_{l,l'} d^{N-M} e^{-\beta E_{l,M}} / Z, \quad (\text{S19})$$

with $\hat{\rho} = Z^{-1} \exp(-\beta H_N)$, $Z = \text{Tr} \exp(-\beta H_N) = \sum_{M=M_0}^N \sum_l d^{N-M} e^{-\beta E_{l,M}}$, and $\beta = 1/k_B T$.

We seek to calculate the von Neumann entanglement entropy S_e with respect to the partition of the system into a subsystem A consisting of the impurity and Wilson chain sites $n = 0, 1, \dots, L-1$ and a subsystem B made up of the remainder of the Wilson chain; see Fig. 1(b) of the main text. Tracing out the degrees of freedom in subsystem B yields the reduced density matrix

$$\rho_A = \text{Tr}_B(\rho) = \begin{pmatrix} \rho_{M_0} & 0 & 0 & 0 \\ 0 & \rho_{M_0+1} & 0 & 0 \\ & & \ddots & \\ 0 & 0 & \rho_L & 0 \\ 0 & 0 & 0 & R_L^{\text{red}} \end{pmatrix}, \quad (\text{S20})$$

where R_M^{red} is the *partial* reduced density matrix with elements $R_M^{\text{red}}(k, k')$ indexed by states k and k' *kept* (not discarded) after iteration M . R_M^{red} can be obtained from R_{M+1}^{red} via reverse iteration along the Wilson chain starting at $M = N-1$, as detailed in Eq. (30) of Ref. 36. Diagonalization of R_L^{red} yields n_L^{kept} eigenvalues of ρ_A that can be combined with the values $(\rho_M)_{ll}$ for $M_0 \leq M \leq L$ to construct the full set of eigenvalues $\{\lambda_a\}$. Finally, one can compute the entanglement entropy

$$S_e = -\text{Tr}_A(\rho_A \ln \rho_A) = -\sum_a \lambda_a \ln \lambda_a. \quad (\text{S21})$$

B. Extraction of a characteristic temperature scale T^*

Figure 4 of the main paper shows that for $r > 0$, the entanglement entropy in each phase (Kondo and local-moment) scales as a function of R/R^* , where $R^* = 1/(k_F T^*)$. For the purposes of this figure, we have extracted the characteristic scale T^* for any $J \neq J_c$ from the temperature dependence of $\chi_{\text{imp}}(T)$, the impurity contribution to the uniform magnetic susceptibility. We define $4T^*$ to be the temperature at which $T\chi_{\text{imp}}$ reaches the midpoint between its critical value (the one that persists to $T=0$ at $J=J_c$) and its zero-temperature limit [4] of $1/4$ (for $J < J_c$) or $r/8$ (for $J > J_c$). This temperature is taken to be $4T^*$ (rather than T^* , say) so that for $r \rightarrow 0^+$ where $4T^*\chi_{\text{imp}}(4T^*) \rightarrow 0.125$, T^* smoothly approaches the metallic ($r=0$) Kondo temperature, normally given the empirical definition $T_K \chi_{\text{imp}}(T_K) = 0.0701$ [12].

C. Entanglement entropy as a function of Kondo coupling J

The main paper presents results for $S_e^{\text{imp}}(J, L)$, the smoothed (three-point-averaged) impurity contribution to the entanglement entropy as a function of the Wilson chain partition size L for different fixed Kondo couplings $\rho_0 J$. Figure S6 instead plots S_e^{imp} vs $\rho_0 J$ for the metallic case $r=0$ with each data set representing a different fixed partition size L . With increasing J , each partition shows a monotonic decrease of S_e^{imp} . For very weak Kondo couplings $\rho_0 J \ll 1$, the impurity spin is collectively screened by essentially the entire Wilson chain. The amount of screening that takes place within the first L sites of the Wilson becomes ever smaller as $J \rightarrow 0^+$, so the impurity's entanglement with chain sites $n \geq L$ approaches the full value $\ln 2$ for a spin singlet.

For the opposite limit $\rho_0 J \gg 1$, in the ground state of H_N given by Eqs. (S3) and (S4), the impurity is essentially locked into a spin singlet with the on-site combination of conduction electrons annihilated by the $f_{0\sigma}$ operator; chain sites $1, 2, \dots, N-1$ behave like a free Wilson chain partitioned into segments of length $L-1$ and $N-L$. As a result, the impurity contribution to the entanglement entropy can be written $S_e^{\text{imp}}(J, L, N) = S_e(J, L, N) - S_e^{(0)}(L, N) \simeq S_e^{(0)}(L-1, N-1) - S_e^{(0)}(L, N)$, where $S_e^{(0)}$ is the entanglement entropy of a chain of length N partitioned into L and $N-L$ sites. After making N very large and performing a three-point average, the smoothed impurity entanglement entropy $S_e^{\text{imp}}(J, L)$ defined in the main paper is negative for $L \lesssim L_\Lambda$ —over which range $S_e^{\text{avg}}(L, N \gg L/2)$ grows with increasing L —and rapidly approaches zero for $L \gtrsim L_\Lambda$. For the value $\Lambda=3$ used to produce Fig. S6, $L_\Lambda \simeq 1$ and negative S_e^{imp} values are found only for $L \lesssim 3$.

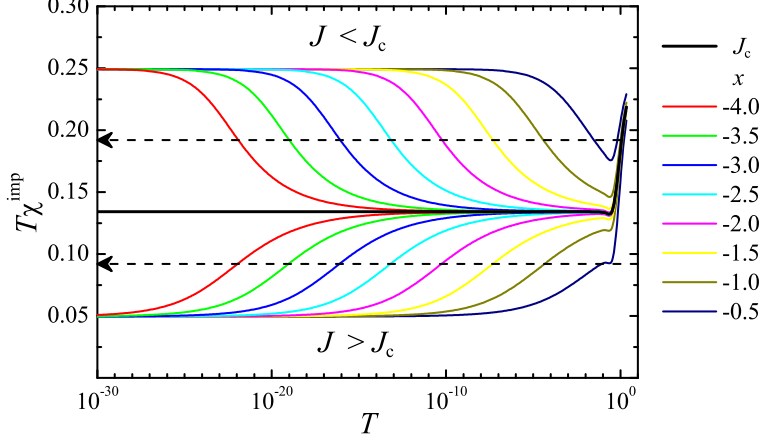


FIG. S5. Extraction of the characteristic temperature scale T^* from $\chi_{\text{imp}}(T)$, the impurity contribution to the uniform magnetic susceptibility. For each value of J , $4T^*$ is defined to be the temperature at which $T\chi_{\text{imp}}(T)$ (solid curves thin solid lines) reaches the midpoint (horizontal dashed line) between its $T \rightarrow 0$ limiting value for that J (namely, $1/4$ for $J < J_c$, $r/8$ for $J > J_c$) and the corresponding limiting value for $J = J_c$ (solid line). Data shown are for band exponent $r = 0.4$ and $J = (1 \pm 10^x)J_c$ with the values of x shown in the legend.

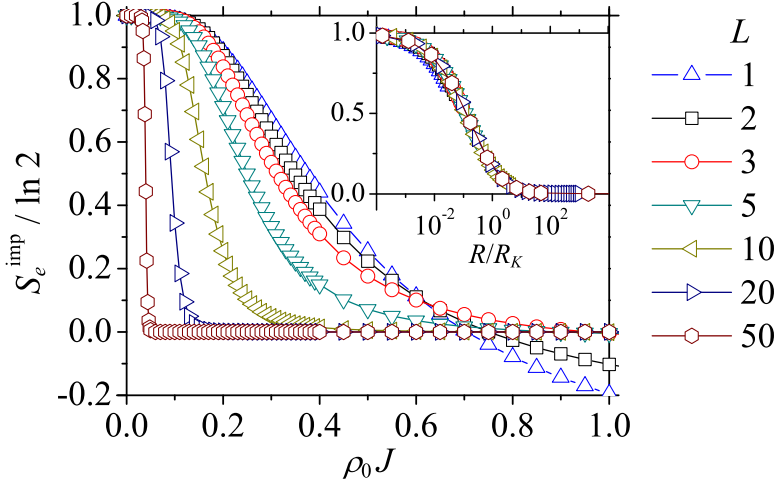


FIG. S6. Impurity entanglement entropy S_e^{imp} vs dimensionless Kondo coupling $\rho_0 J$ for band exponent $r = 0$, discretization parameter $\Lambda = 3$ and different partition sizes L . The inset shows the collapse of curves for different L values when the data spanning $\rho_0 J \leq 0.3$ are replotted as S_e^{imp} vs R/R_K .

As L is increased, the crossover in S_e^{imp} from $\ln 2$ toward zero takes place more sharply and centered around a smaller value of $\rho_0 J$. This is another manifestation of the notion presented in the main text that S_e^{imp} drops once the radius R of subsystem A exceeds the characteristic size R_K of the Kondo screening cloud. The inset of Fig. S6 replots the data for $\rho_0 J \leq 0.3$ as a function of R/R_K , where each L curve corresponds to fixed value of $R = c\Lambda^{L/2}/k_F$ (with k_F being the Fermi wave vectors and c a constant of order unity) and points within a curve arise from a decrease with increasing J of $R_K \sim 1/(k_F T_K)$. Whereas in the main paper, the Kondo temperature T_K was deduced from the impurity contribution to the magnetic susceptibility via the conventional definition $T\chi_{\text{imp}}(T_K) = 0.0701$ [12], in Fig. S6 we instead employed the perturbative definition [13]

$$k_B T_K \sim D \sqrt{\rho_0 J} \exp[-1/(\rho_0 J) + O(\rho_0 J)]. \quad (\text{S22})$$

The collapse of all curves except those for $L = 1$ and 2 (which are anomalous for reasons discussed in the preceding paragraph) is consistent with the existence of a universal scaling function $S_e^{\text{imp}}(J, R) = f_0(R/R_K)$, as also argued on the basis of the data presented in the main paper.

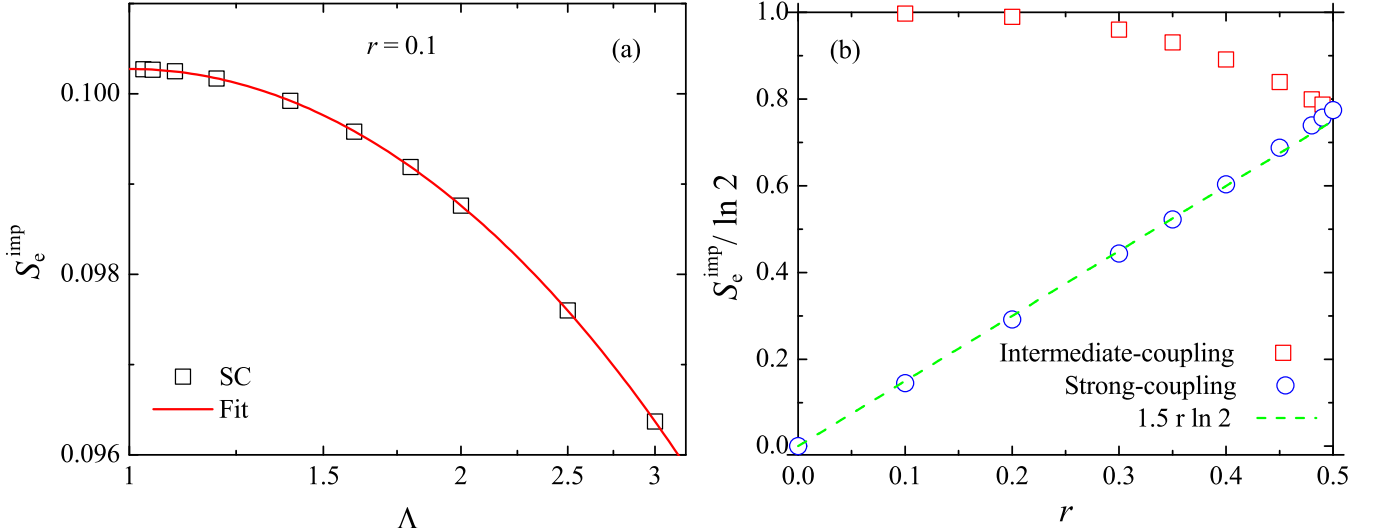


FIG. S7. Impurity entanglement at the quantum critical point and the Kondo fixed point: (a) Kondo fixed-point value of S_e^{imp} (symbols) vs Λ (on a log scale) for band exponent $r = 0.1$. A polynomial fit (solid line) is used to extrapolate S_e^{imp} to the continuum limit $\Lambda = 1$. (b) Extrapolated $\Lambda = 1$ values of S_e^{imp} at the critical point (squares) and at the Kondo fixed point (circles) vs band exponent r , along with a heuristic fit $S_e^{\text{imp}} = \frac{3}{2}r \ln 2$ (dashed line).

Similar behavior can be seen in plots (not shown) of S_e^{imp} vs $\rho_0 J$ at fixed L for pseudogapped hosts (i.e., $r > 0$). The data in each phase (Kondo or local-moment) can be collapsed by plotting S_e^{imp} against R/R^* , where the crossover length scale $R^* = 1/k_F T^*$. While T^* can be determined from $\chi_{\text{imp}}(T)$ via the operational procedure laid out in Sec. II B, for values of J sufficiently close to J_c , good collapse can be achieved by instead using the asymptotic expression

$$T^* \propto |J - J_c|^\nu, \quad (\text{S23})$$

where the numerical value of the correlation length exponent ν has a nontrivial dependence on the band exponent r [14].

D. Fixed-point entanglement entropy vs r

This section provides more details of the r dependence of the impurity entanglement entropy at each renormalization-group fixed point, as well as the manner in which S_e^{imp} approaches its value at each of the stable fixed points.

The results in the main paper show that, whereas $S_e^{\text{imp}} = 0$ at the weak-coupling fixed point, the impurity entanglement entropy takes nontrivial, r -dependent values at the Kondo-destruction quantum critical point and at the Kondo fixed point. The fixed-point values of S_e^{imp} can be obtained from many-body NRG calculations by taking the limit $R \ll R^*$ (for the unstable critical point) or $R \gg R^*$ (for the stable Kondo and local-moment fixed points). The Kondo fixed-point value of S_e^{imp} can also be calculated using the single-particle method outlined in Sec. I B as the difference of S_e^{avg} for a free Wilson chain with and without the first site frozen due to the formation of a local spin singlet with the magnetic impurity. That the many-body and single-particle approaches yield numerical values in excellent agreement provides a valuable check on the accuracy of the full NRG results.

In order to remove discretization effects, fixed-point values of S_e^{imp} were calculated for values of Λ between 1.01 and 3, then fitted with a polynomial function of $\ln \Lambda$, allowing extrapolation of S_e^{imp} to the continuum limit $\Lambda = 1$, as illustrated in Fig. S7(a).

Extrapolated values of S_e^{imp} are shown in Fig. S7(b). As r increases from 0, the critical value of S_e^{imp} decreases from $\ln 2$ while the Kondo fixed-point value increases almost linearly from 0. The two fixed-point values meet at $r = \frac{1}{2}$, the band exponent at which the quantum critical point merges with the Kondo fixed point. (No quantum critical point exists for $r > \frac{1}{2}$ [4].) A weak superlinear variation can be seen when the Kondo entanglement entropy is compared with a heuristic fit $S_e^{\text{imp}} = \frac{3}{2}r \ln 2$ [dashed line in Fig. S7(b)]. This superlinear behavior is somewhat unexpected since thermodynamic properties at strong coupling have been shown to exhibit a strictly linear variation with r [4].

r	$\alpha(\text{LM})$	$\alpha(\text{K})$
0.0	0	1.000(3)
0.2	0.38(3)	0.800(5)
0.25		0.750(4)
0.3	0.58(5)	0.693(8)
0.33		0.630(7)
0.4	0.79(4)	0.399(5)
0.45	0.89(5)	0.199(2)
0.5	1	0

TABLE II. Values of the exponent α defined in Eq. (S24) for different band exponents r , as determined in the local-moment (LM) and Kondo (K) phases. A number in parentheses denotes the estimated nonsystematic error in the last digit. Values without error estimates are assumed rather than computed.

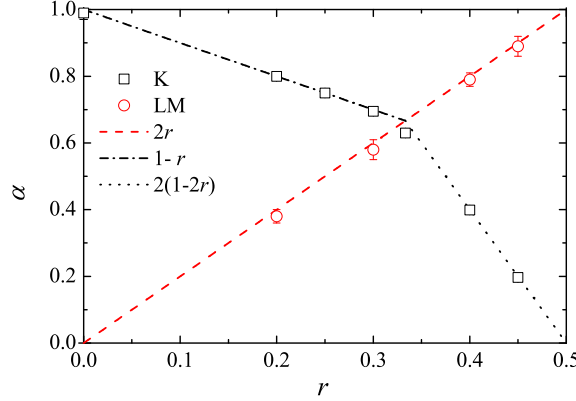


FIG. S8. Values of the exponent α defined in Eq. (S24) for different band exponents r , as determined in the local-moment (LM, circles) and Kondo (K, squares) phases, along with lines showing the functions $\alpha = 2r$, $1 - r$, and $2(1 - 2r)$.

Insets in Fig. 4 of the main paper demonstrate that S_e^{imp} has a power-law-decaying tail in both the local-moment and Kondo phases, namely,

$$S_e^{\text{imp}}(J, R) - S_e^{\text{imp}}(J, \infty) \propto (R/R^*)^{-\alpha} \quad \text{for } R \gg R^*. \quad (\text{S24})$$

Fitted values of α are listed in Table II and plotted in Fig. S8. To within the estimated numerical uncertainty, the extracted exponents are consistent with $\alpha = 2r$ for $J < J_c$ and $\alpha = \min(1 - r, 2 - 4r)$ for $J > J_c$. These expressions coincide with twice the exponent of the leading irrelevant operator at the local-moment and Kondo fixed points, respectively; see Eqs. (4.7) and (4.10) in Ref. 14. This is consistent with the natural interpretation that the power-law tails are associated with the renormalization-group flow toward the stable fixed point in either phase, leading to the expectation that the exponent α is a characteristic of that fixed point.

It is probable that the departure of S_e^{imp} from its value on the critical plateau is also described by a power-law behavior, i.e.,

$$S_e^{\text{imp}}(J, R) - S_e^{\text{imp}}(J_c, \infty) \propto (R/R^*)^{\alpha'} \quad \text{for } R \ll R^*, \quad (\text{S25})$$

where one would expect α' to be positive and a characteristic property of the Kondo destruction critical point (and, hence, likely to have a nontrivial r dependence). However, numerical uncertainty in the value of the critical value $S_e^{\text{imp}}(J_c, \infty)$ impedes reliable determination of α' .

[1] K. G. Wilson, Rev. Mod. Phys. **47**, 773 (1975).

[2] R. Bulla, T. A. Costi, and T. Pruschke, Rev. Mod. Phys. **80**, 395 (2008).

- [3] In the presence of particle-hole asymmetry [i.e., if it is not true that $\rho(\varepsilon) = \rho(-\varepsilon)$ for all ε], then the right-hand side of Eq. (S2) must be supplemented by on-site term $\sum_{n=0}^N \sum_{\sigma} \varepsilon_n f_{n\sigma}^\dagger f_{n\sigma}$, where $|\varepsilon_n|$ decays exponentially with n for $n \gg 1$.
- [4] C. Gonzalez-Buxton and K. Ingersent, Phys. Rev. B **57**, 14254 (1998).
- [5] I. Peschel, J. Phys. A: Math. and Theor. **36**, L205 (2003).
- [6] P. Calabrese and J. Cardy, J. Stat. Mech: Theor. and Exp. **2004**, P06002 (2004).
- [7] A. Weichselbaum and J. von Delft, Phys. Rev. Lett. **99**, 076402 (2007).
- [8] L. Merker, A. Weichselbaum, and T. A. Costi, Phys. Rev. B **86**, 075153 (2012).
- [9] H. T. M. Nghiêm and T. A. Costi, Phys. Rev. B **90**, 035129 (2014).
- [10] F. B. Anders and A. Schiller, Phys. Rev. Lett. **95**, 196801 (2005).
- [11] F. B. Anders and A. Schiller, Phys. Rev. B **74**, 245113 (2006).
- [12] H. R. Krishna-murthy, J. W. Wilkins, and K. G. Wilson, Phys. Rev. B **21**, 1003 (1980).
- [13] A. C. Hewson, *The Kondo Problem to Heavy Fermions* (Cambridge Univ. Press, Cambridge, UK, 1993).
- [14] K. Ingersent and Q. Si, Phys. Rev. Lett. **89**, 076403 (2002).